

CZECH TECHNICAL UNIVERSITY IN PRAGUE
Faculty of Nuclear Sciences and Physical
Engineering

Department of Physics



Research project

**Preparation of the HFT detector for the STAR
experiment**

Bc. Michal Tesař

Supervisor: Mgr. Jaroslav Bielčík, PhD.

Praha 2009

Contents

List of Figures	iii
List of Tables	iv
Preface	1
1 Physical background	2
2 Detector design	3
3 Analysis of simulated Au+Au events at $\sqrt{s_{NN}} = 200$ GeV	5
3.1 D ⁺ reconstruction	5
3.2 Control plots	6
3.3 Reconstruction efficiency	8
3.4 DCA resolution	8
4 D ⁺ signal significance	14
4.1 Rescaling of results to 100M events	14
4.2 Cut optimization	15
4.3 Results	15
Conclusions	19
Bibliography	21

List of Figures

2.1	Geometry of silicon detectors of STAR tracking system	4
2.2	PIXEL detector with its support structure	4
3.1	D ⁺ decay diagram	6
3.2	D ⁺ distribution in $p_T - \eta$ plane for Monte Carlo particles	7
3.3	D ⁺ distribution in $p_T - \eta$ plane for reconstructed particles	8
3.4	D ⁺ distribution in $p_T - \varphi$ plane for Monte Carlo particles	9
3.5	D ⁺ distribution in $p_T - \varphi$ plane for reconstructed particles	9
3.6	D ⁺ decay length vs. D ⁺ momentum for Monte Carlo particles	10
3.7	D ⁺ decay length distribution for Monte Carlo particles	10
3.8	Reconstruction probability of pion and kaon tracks	11
3.9	D ⁺ reconstruction efficiency under various conditions	12
3.10	DCA resolution in X-Y plane for pion and kaon	13
3.11	DCA resolution in Z-direction for pion and kaon	13
4.1	D ⁺ signal and background before rescaling and significance after rescaling to 100M events.	16
4.2	Expected D ⁺ signal for 100M central Au+Au collisions at $\sqrt{s_{NN}} = 200$ GeV, $0.5 < p_T < 1.0$ eV/c	17
4.3	Expected D ⁺ signal for 100M central Au+Au collisions at $\sqrt{s_{NN}} = 200$ GeV, $1.0 < p_T < 1.5$ GeV/c	17
4.4	Expected D ⁺ signal for 100M central Au+Au collisions at $\sqrt{s_{NN}} = 200$ GeV, $1.5 < p_T < 2.0$ GeV/c	18

List of Tables

2.1	Radius and hit position resolution of SSD and HFT layers.	3
3.1	Summary of used cuts and their values.	6
4.1	D ⁺ signal significance	19

Preface

The Heavy Flavor Tracker (HFT), a new inner tracking detector for the STAR experiment, is now in development. Its main purpose is to improve capabilities to measure production, displaced vertices and do the direct topological reconstruction of charm and bottom hadrons and thus study the heavy flavor quark production in heavy-ion collisions. The main physics motivation is in partonic energy loss, flow and tests of thermalization of the hot and dense nuclear matter.

The HFT consists of two groups of different detectors. The outer layer is formed of a single-sided strip detector, the Intermediate Silicon Tracker (IST). The two inner layers are made of the PIXEL detector. PIXEL uses monolithic active pixel sensors (MAPS), which are fabricated by CMOS technology. This approach will provide to make the detector extremely thin. Thanks to this feature HFT will be capable to reconstruct heavy flavor mesons even for low p_T , which makes it unique.

This work investigates capabilities of the current design of the HFT to reconstruct D^+ mesons via $D^+ \rightarrow K^- \pi^+ \pi^+$ decay channel. We have studied this topic through Monte Carlo simulations. Our main aim was to maximize the significance of the D^+ signal at low p_T .

Chapter 1

Physical background

Heavy quarks are produced in the early stage of the collision of the nuclei, by hard scattering of partons. Because the amount of produced heavy quarks is not modified in the later stages of the Quark Gluon Plasma (QGP), the heavy quarks carry the information about the initial phase of the collision.

With the use of the heavy quarks we can probe the medium created in ultra-relativistic collisions of heavy ions. Important topic to study is suppression of high p_T hadrons and jet quenching. These are believed to be caused by partonic energy loss. The energy loss of heavy quarks compared to light quarks is predicted to be smaller due to the “dead cone” effect¹ [1]. For further studies precise measurements [2] of nuclear modification factor R_{AA} should be done.

It was revealed that partons in heavy ion collisions show collective expansion. However, it is not clear whether the thermalization of the hot matter takes place. More accurate measurement of elliptic flow v_2 of charmed hadrons will shed light on this question. If the flow of heavy flavor and light flavor hadrons showed the same pattern, it would indicate frequent interactions between light and heavy quarks and thus thermalization in the early stages of the collision.

Most of present analyses at STAR dealing with heavy flavors use electrons which arise from leptonic and semileptonic decays of heavy flavor hadrons. Because of the escaping neutrinos the kinematical information is incomplete and it is difficult to study previously mentioned quantities at low p_T . Furthermore, electron originating from b and c quarks cannot be distinguished without displaced vertex measurement. That is why the direct topological reconstruction of open charm hadrons via hadronic decay modes is needed. HFT is proposed to reconstruct displaced vertices of open charm hadrons and improve signal significance.

¹gluon radiation is suppressed at angles $\Theta < M_Q/E$, M_Q - quark mass, E - quark energy

Chapter 2

Detector design

The HFT detector [3] is placed inside the STAR detector very close to the beam pipe. It consists of two detector systems and it has 2π azimuthal and ± 1.0 pseudorapidity coverage. The main purpose is to reconstruct displaced vertices of heavy flavor mesons with precision about $50 \mu\text{m}$.

This resolution can be achieved by use of low-mass monolithic active pixel sensors (MAPS) fabricated by CMOS technology. This part of the detector is called PIXEL detector and consists of two layers (see Fig. 2.2). Because of the small thickness the beam pipe ($0.15\% X_0$) and the detector with its support structure ($0.37\% X_0$ per layer), production of e^+e^- pairs from photon conversions and multiple Coulomb scattering will be reduced.

The second subsystem is the Intermediate Silicon Tracker (IST), a single-sided fast strip detector. Its task is to improve pointing resolution of the tracks reconstructed in Time Projection Chamber (TPC) in the high-multiplicity environment of heavy ion collisions. For parameters of the silicon detectors see Tab. 2.1.

Other detectors employed in the midrapidity tracking system of STAR are TPC and the Silicon Strip Detector (SSD). Geometry of mentioned silicon detectors is shown in Fig. 2.1.

layer	$r[\text{cm}]$	hit resol. ($r - \phi \times z$) [$\mu\text{m} \times \mu\text{m}$]
SSD	23	30×699
IST	14	115×2900
PIXEL2	8	5×5
PIXEL1	2.5	5×5

Table 2.1: Radius and hit position resolution of SSD and HFT layers.

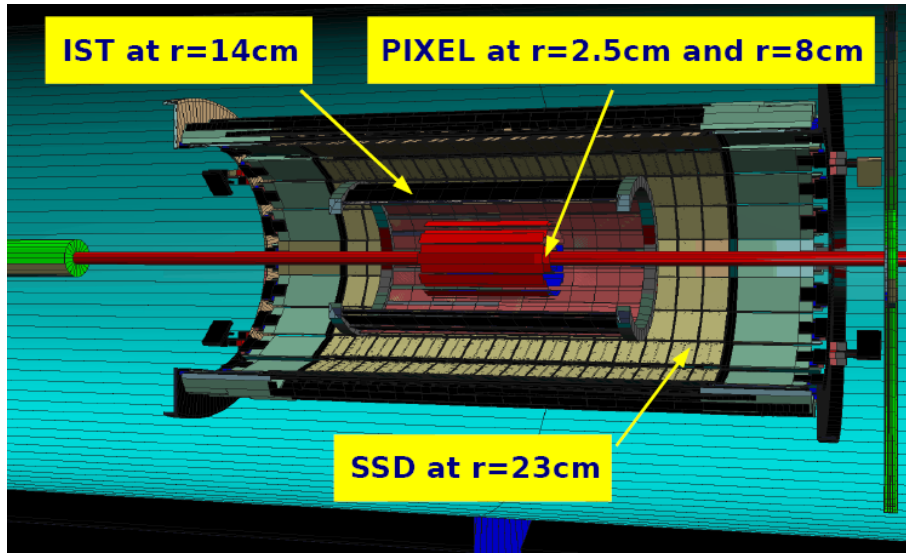


Figure 2.1: Geometry of silicon detectors of STAR tracking system; both subsystems of the HFT (PIXEL and IST) and existing SSD.

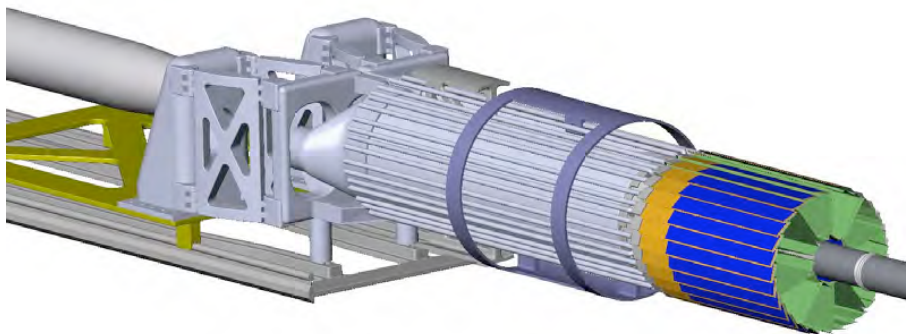


Figure 2.2: PIXEL1 and PIXEL2 layers (blue pads) with their support structure.

Chapter 3

Analysis of simulated Au+Au events at $\sqrt{s_{NN}} = 200 \text{ GeV}$

The data set used for analysis was 10 000 Au+Au HIJING generated events. Centrality of the simulated collisions is 0-10% and collision energy $\sqrt{s_{NN}} = 200 \text{ GeV}$. In each event were embedded five D^+ with uniform p_T distribution from 0 to 10 GeV/c. Particles from HIJING and D^+ were filtered through GEANT model of the STAR detector with HFT upgrade (“upgr15”) and detector response was simulated.

3.1 D^+ reconstruction

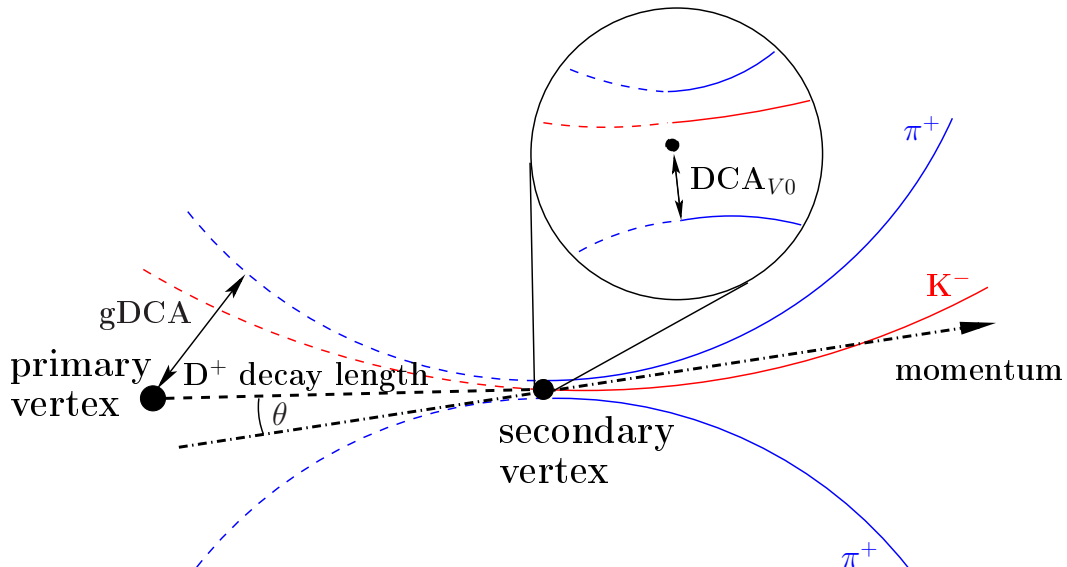
In the analysis we are looking for D^+ mesons [4] ($1869 \text{ MeV}/c^2$), having $c\tau = 312 \mu\text{m}$. We use the $D^+ \rightarrow K^- \pi^+ \pi^+$ (B.R. 9.5%) decay channel, hence we have to survey all possible triplets $K^- \pi^+ \pi^+$. However, not all of these triplets come from D^+ decays and if we considered all the triplets, their number would be enormous. To reduce the background we use in all analyses concerning D^+ following set of cuts, values of some of them were further optimized (see section 4.2).

Distance of closest approach (DCA) of daughter particles (pions and kaons) to the primary vertex (global DCA cut) has to be greater than $100 \mu\text{m}$. On DCA of daughters to the D^+ vertex (DCA_{V0}) we put condition $DCA_{V0}/resolution < 2$, where *resolution* is pointing resolution of current particle type. The pions and the kaons also have to have reconstructed hits in both PIXEL layers and 15 hits in TPC. Next cut is $\cos \theta > 0.99$, where θ is the angle between the join of primary and secondary vertex and $K^- \pi^+ \pi^+$ triplet momentum. These cuts are illustrated in D^+ decay diagram (Fig. 3.1). Invariant mass¹ of the triplet we require to be between 1819 and 1919 MeV/c^2 . From all events we took only those ones, which have the primary vertex highly 5 cm away from center of the detector in Z-direction. Values of used cuts are summarized in Tab. 3.1

¹ $(M_{inv}c)^2 = (\sum_i E_i)^2 - \|\sum_i \vec{p}_i c\|^2$, where the sums are over all particles.

quantity	range
inv. mass [MeV/c ²]	1819 - 1919
global DCA [μm]	> 100
DCA _{V0} /resol.	< 2
cos θ	> 0.99
vertex Z pos. [cm]	± 5

Table 3.1: Summary of used cuts and their values.

Figure 3.1: D^+ decay diagram. ($D^+ \rightarrow K^- \pi^+ \pi^+$)

3.2 Control plots

To check correctness of the data, whether they are generated as expected, we made a set of control plots. Fig. 3.2 shows D^+ distribution in $p_T - \eta$ plane² for the Monte Carlo (MC) simulated particles. The region $|\eta| < 1$ and $0 < p_T < 10$ GeV/c represents the embedded D^+ , the rest comes from HIJING. It is clear that the $p_T - \eta$ distribution of embedded D^+ is flat as it should be.

The same plot, but for the reconstructed D^+ is in Fig. 3.3. Reconstructed means that the tracks of daughter particles were correctly reconstructed in the tracker. The density as well as the number of entries has dropped significantly and all D^+ outside the $|\eta| < 1$ region vanished due to detector acceptance. Lower density for low p_T is due to multiple Coulomb scattering (MCS), because the tracks of the scattered particles are incorrectly reconstructed.

Very similar to the previous plots are Fig. 3.4 and Fig. 3.5, which show D^+

² p_T - transverse momentum, compound of particle momentum perpendicular to beam direction;
 η - pseudorapidity, $\eta = -\ln[\tan(\theta/2)]$

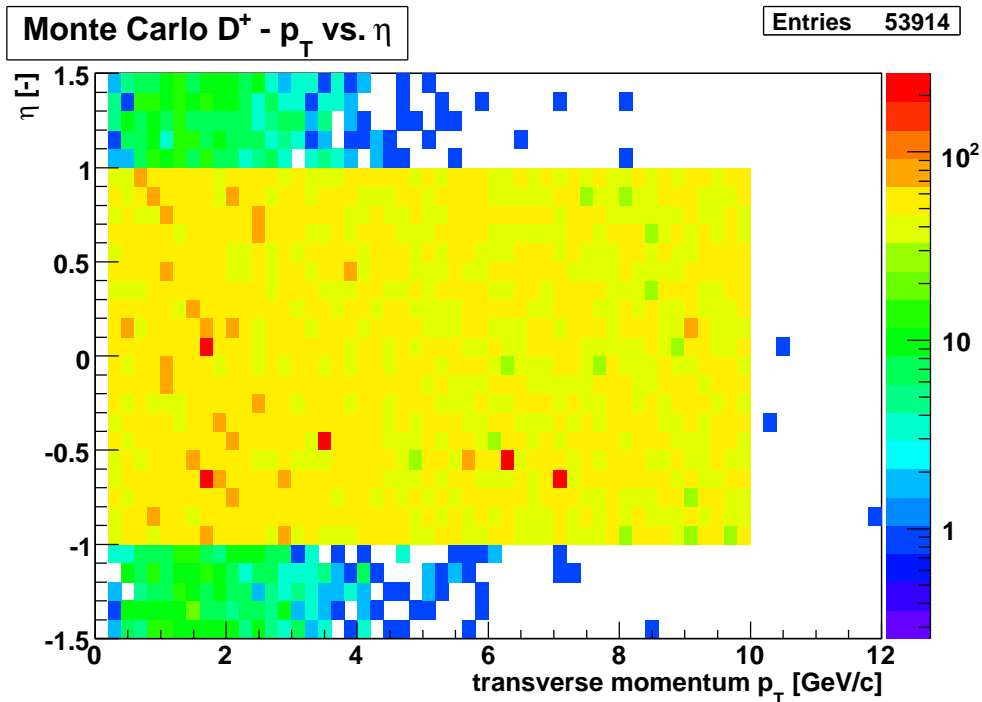


Figure 3.2: D^+ distribution in $p_T - \eta$ plane for Monte Carlo particles. (No cuts applied.)

distribution in $p_T - \varphi$ plane³ for the Monte Carlo and reconstructed particles, respectively. In Fig. 3.4 we see that the distribution is flat too, hence the whole spacial D^+ distribution is isotropic. Higher D^+ density in low p_T region we set down to the HIJING background (in $|\eta| > 1$ region). In Fig. 3.5 this low p_T region turns into low density due to limited detector acceptance in η and MCS. In the plot for reconstructed particles number of entries falls down again.

Further we checked, if D^+ decay length as a function of momentum has correct shape (see Fig. 3.6). In this figure is shown the dependency for Monte Carlo particles (crosses). The straight line is a ideal linear function of this relation.

Next plot (Fig. 3.7) is a histogram of distribution of decay lengths of D^+ in logarithmic scale. It is done for D^+ momentum between 1 and 2 GeV/c. It is fitted with an exponential, which describes the data well up to decay lengths of 1500 μm , where the number of decaying D^+ becomes to be very low.

These control plots show character of the simulated data, impact of tracking on the data and mainly prove that the Monte Carlo simulated data as well as the reconstructed data are generated with correct properties.

³ φ - azimuthal angle

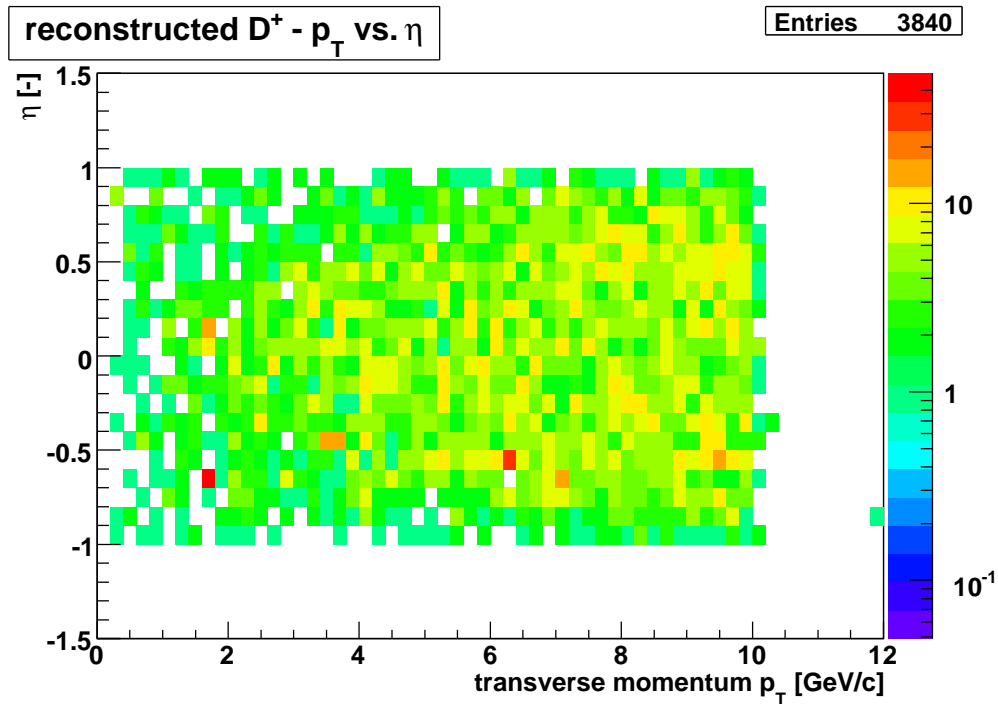


Figure 3.3: D^+ distribution in $p_T - \eta$ plane for reconstructed particles.

3.3 Reconstruction efficiency

Plots Fig. 3.8 and Fig. 3.9 show π and K tracking efficiency as a function of p_T and the efficiency of D^+ reconstruction, respectively. In Fig. 3.8 the tracking efficiency for K is in comparison to π a little bit lower due to its higher mass (and thus MCS) and shorter lifetime. For this probability calculation we require correctly associated hits in both PIXEL layers and 15 hits in TPC.

For D^+ (Fig. 3.9), the efficiency is calculated for three cases, i. e. after successful tracking of D^+ daughters, after tracking with use of the gDCA cut (see section 3.1) and after tracking with use of the gDCA cut plus the best significance cuts for $1.0 < p_T < 1.5$ GeV/c (more in section 4.2). The reconstruction efficiency for D^+ is smaller than for D^0 [5], because in D^+ case is one needs to reconstruct three daughter tracks with lower p_T than in two body decay case.

3.4 DCA resolution

Other important parameter of the detector is its pointing resolution to primary vertex for different particles. Thereby we show the DCA (to primary vertex) resolution in X-Y plane (Fig. 3.10) and in Z-direction (Fig. 3.11) for π and K.

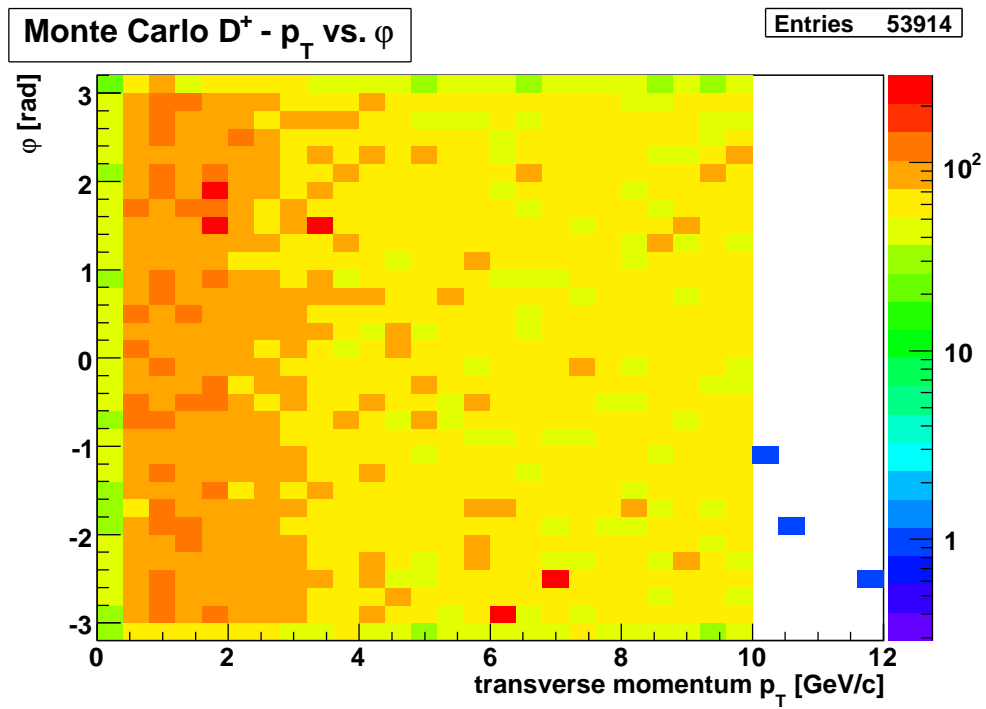


Figure 3.4: D^+ distribution in p_T - ϕ plane for Monte Carlo particles. (No cuts applied.)

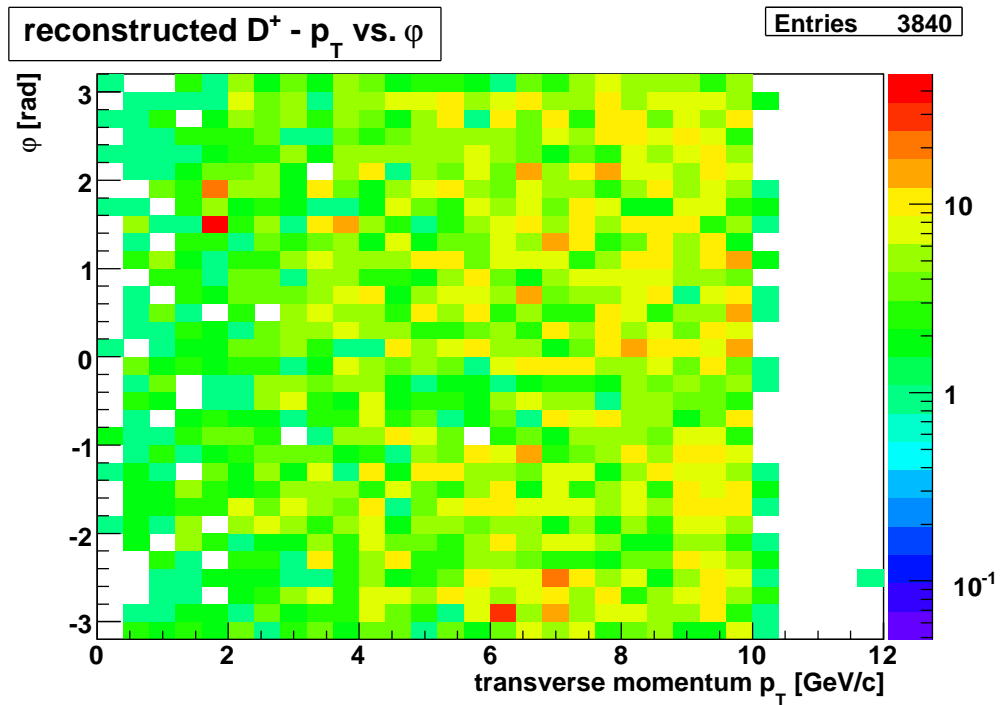


Figure 3.5: D^+ distribution in p_T - ϕ plane for reconstructed particles.

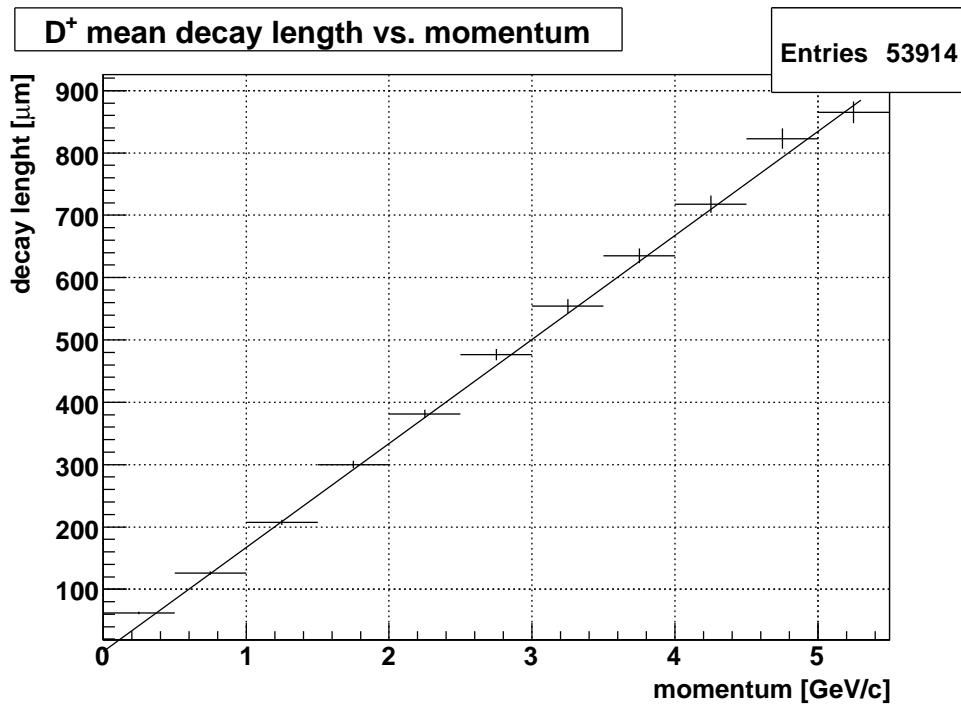


Figure 3.6: D⁺ decay length as a function of its momentum for Monte Carlo particles. (No cuts applied.)

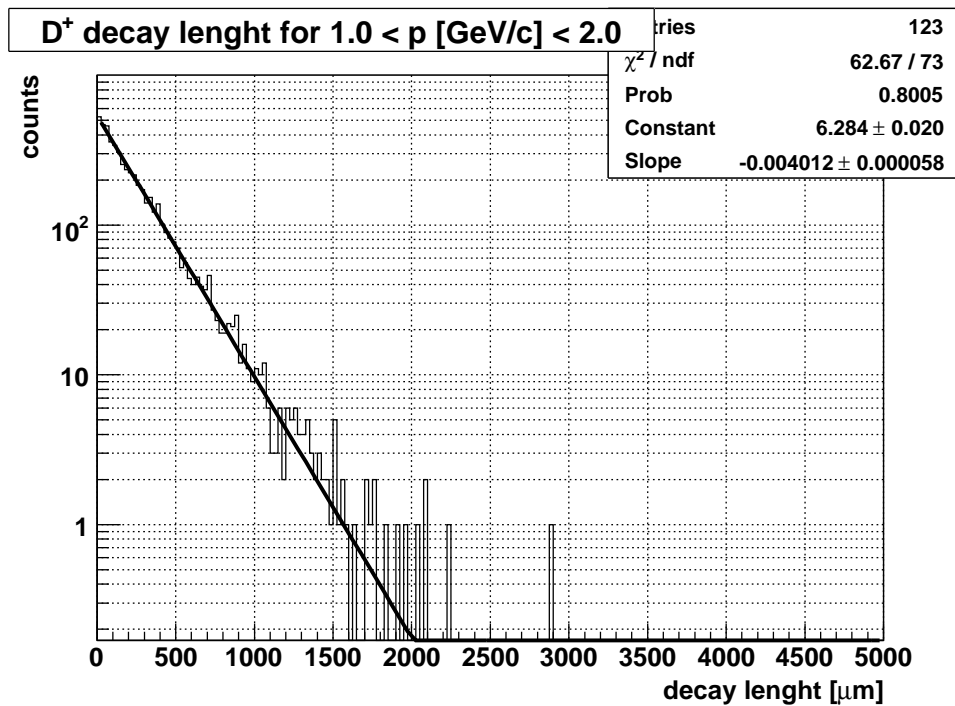


Figure 3.7: D⁺ decay length distribution fitted with exponential for Monte Carlo particles. (No cuts applied.)

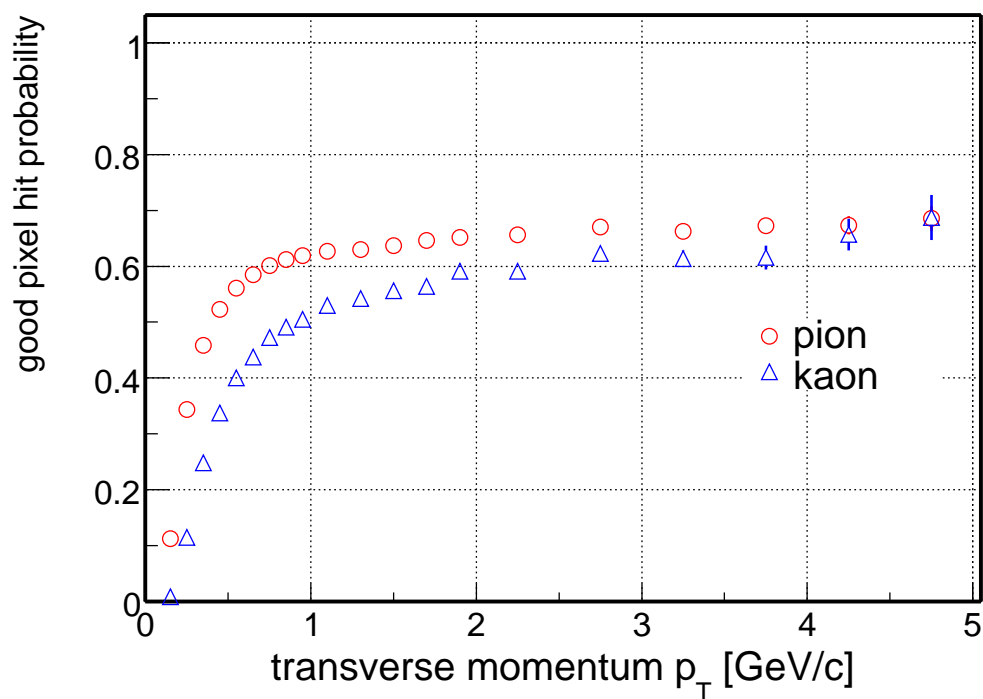


Figure 3.8: Reconstruction probability of pion and kaon tracks. (Requirements: $|\eta| < 1$, correctly associated hits in both PIXEL layers, 15 hits in TPC.)

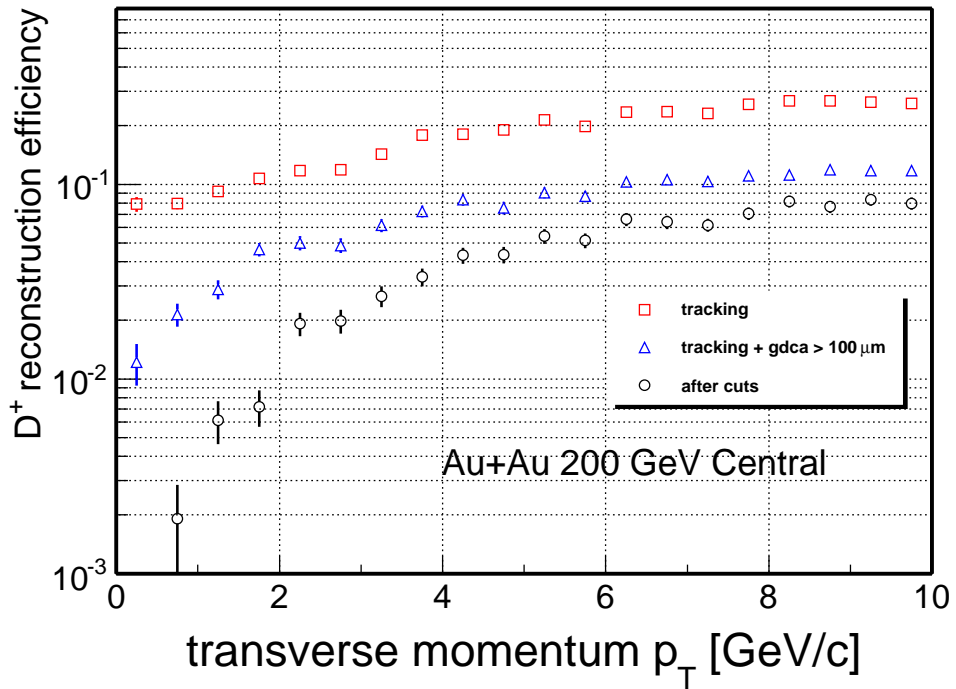


Figure 3.9: D^+ reconstruction efficiency after successful tracking of D^+ daughters and after applying cuts ($1819 < M_{inv} < 1919$ MeV/ c^2 , $gDCA > 115$ μm , $\cos\theta > 0.997$, $DCA_{V0}/resol. < 2$. Requirement of good PID, that limits D^+ acceptance to $p_T < 4.8$ GeV/ c , is not applied here (more in section 4.2).)

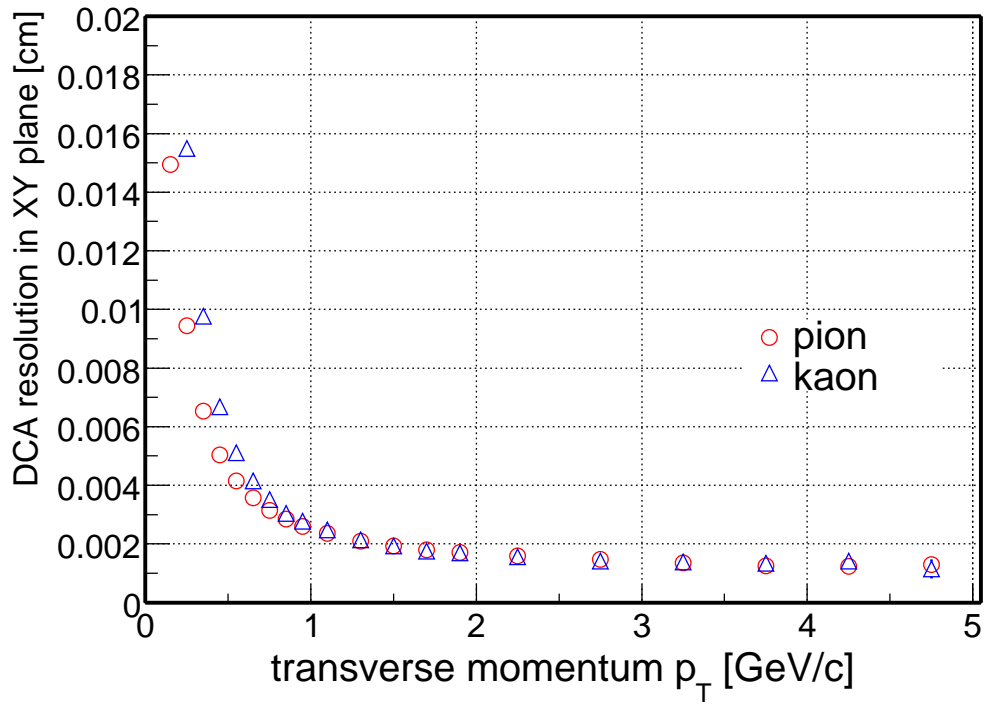


Figure 3.10: DCA resolution in X-Y plane for pion and kaon after tracking. (Requirements: $|\eta| < 1$, correctly associated hits in both PIXEL layers, 15 hits in TPC.)

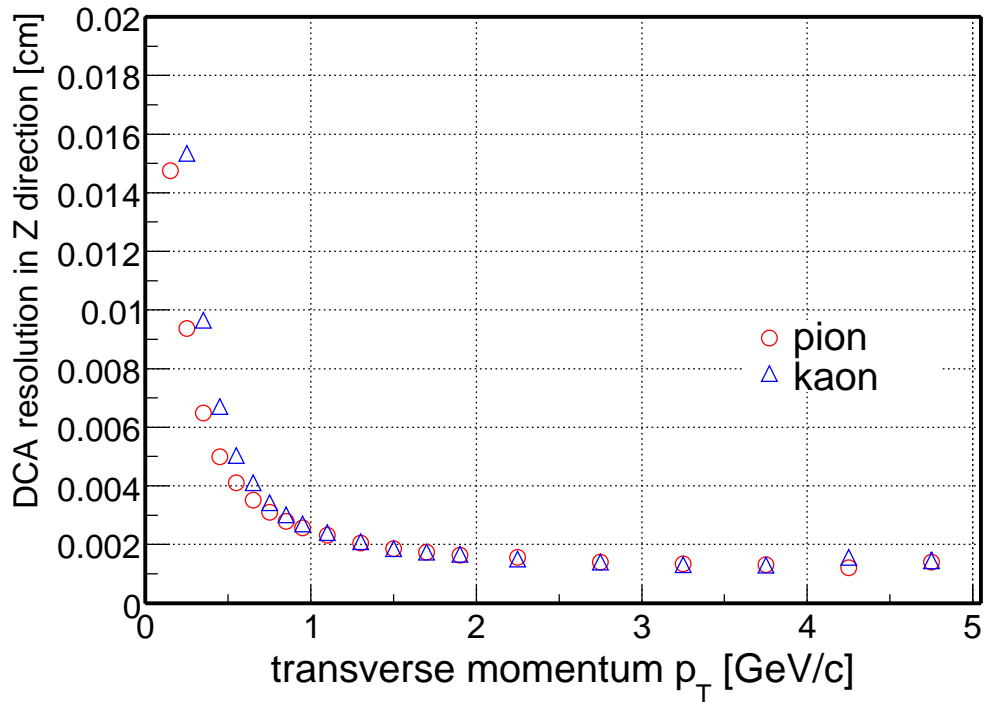


Figure 3.11: DCA resolution in Z-direction for pion and kaon after tracking. (Requirements: $|\eta| < 1$, correctly associated hits in both PIXEL layers, 15 hits in TPC.)

Chapter 4

D⁺ signal significance

The point of this work was to examine D⁺ signal significance under conditions of new HFT design (upgr 15). We analyzed significance up to D⁺ $p_T = 2.0$ GeV/c, which is unique for STAR and HFT.

4.1 Rescaling of results to 100M events

With DAQ 1000 upgrade in STAR (commissioned in 2009), 100 million central Au+Au events will be collected in less than 1 month of operation under realistic conditions (combination with other triggers, detector and RHIC duty factor). Therefore we estimate our significance for 100M central events.

If we have simulated 10 000 Au+Au events and want to get estimates for 100M, the data would have to be rescaled in a proper way. Furthermore, because the number of D⁺ produced per event in the simulation does not correspond real production, the signal has to be divided by following factor:

$$F = \frac{\langle \# D^+ \text{ per unit } \eta \rangle}{\langle \# D^+ \text{ per unit } y \rangle \langle B.R. \rangle} \quad (4.1)$$

In our case the number of D⁺ per unit of η (pseudorapidity) is 2.5 (5 D⁺'s in $|\eta| < 1$), number of D⁺ per unit of y (rapidity¹) is an estimate for central Au+Au collision equal to 0.8, branching ratio is 9.5%. These values give $F = 32.9$.

As mentioned in chapter 3, the p_T distribution of simulated D⁺'s is uniform. It has to be rescaled due to fact, that the p_T spectra of real Au+Au collisions is assumed to be governed by power-law:

$$\frac{1}{p_T} \frac{dN}{dp_T} = C \cdot \left(1 + \frac{p_T}{p_0} \right)^{-n}, \quad (4.2)$$

$$p_0 = \langle p_T \rangle \cdot \frac{n-3}{2}, \quad (4.3)$$

¹ y - rapidity, $y = \text{arctanh}(v/c)$

where C is a normalization constant, $\langle p_T \rangle = 1.0$ GeV/c and $n = 11$.

Beside these rescalings the recomputation from pseudorapidity to rapidity has to be done.

4.2 Cut optimization

To separate signal from background and therefore maximize the significance, we were tuning two earlier mentioned cuts (see section 3.1). We were testing the amount of signal and background for various values of gDCA cut and $\cos\theta$ cut. We obtained the best results if we increase the gDCA cut in discrete steps in range 100 - 235 μm and do the same with $\cos\theta$ cut between 0.990 and 0.999 simultaneously. As a third cut was used narrower $K^-\pi^+\pi^+$ invariant mass window $1854 < M_{inv} < 1884$ MeV/c². For unambiguous particle identification (good PID) we assumed that π and K can be separated for $p_T < 1.6$ GeV/c, this is expected to be achieved with use of the MRPC TOF. For D^+ $p_T < 2$ GeV/c the use of the good PID requirement gives higher significance than if we take also misidentified $p_T > 1.6$ GeV/c particles. Therefore we used the good PID cut for all daughter particles in this computation. All this was done separately for three p_T ranges: 0.5 - 1.0 GeV/c, 1.0 - 1.5 GeV/c and 1.5 - 2.0 GeV/c. We tried to get results for p_T in range 0.0 - 0.5 GeV/c too, but the signal was too small in this interval.

4.3 Results

Tuning of the cuts and the best significance cut are clearly shown in Fig. 4.1. Histograms in horizontal rows in the plot represent amount of D^+ signal before rescaling, amount of background before rescaling and computed D^+ signal significance after rescaling to 100M events. It can be clearly seen for which cut is the significance highest in each p_T interval.

This “significance” is in fact the true significance minus its error, we chose this quantity, because it is more relevant than significance itself. If the significance error was of the same magnitude as significance, the significance itself would be meaningless. Hence significance minus its error brings correct information. We employ this approach because of the limited statistics of our simulation.

In the last three illustrative plots (Fig. 4.2, Fig. 4.3, Fig. 4.4) we show for mentioned p_T ranges, how would the D^+ peak with current significance look like. We repeat that these are results for 100M central Au+Au collisions at $\sqrt{s_{NN}} = 200$ GeV with use of upgr15 of the Heavy Flavor Tracker detector for STAR.

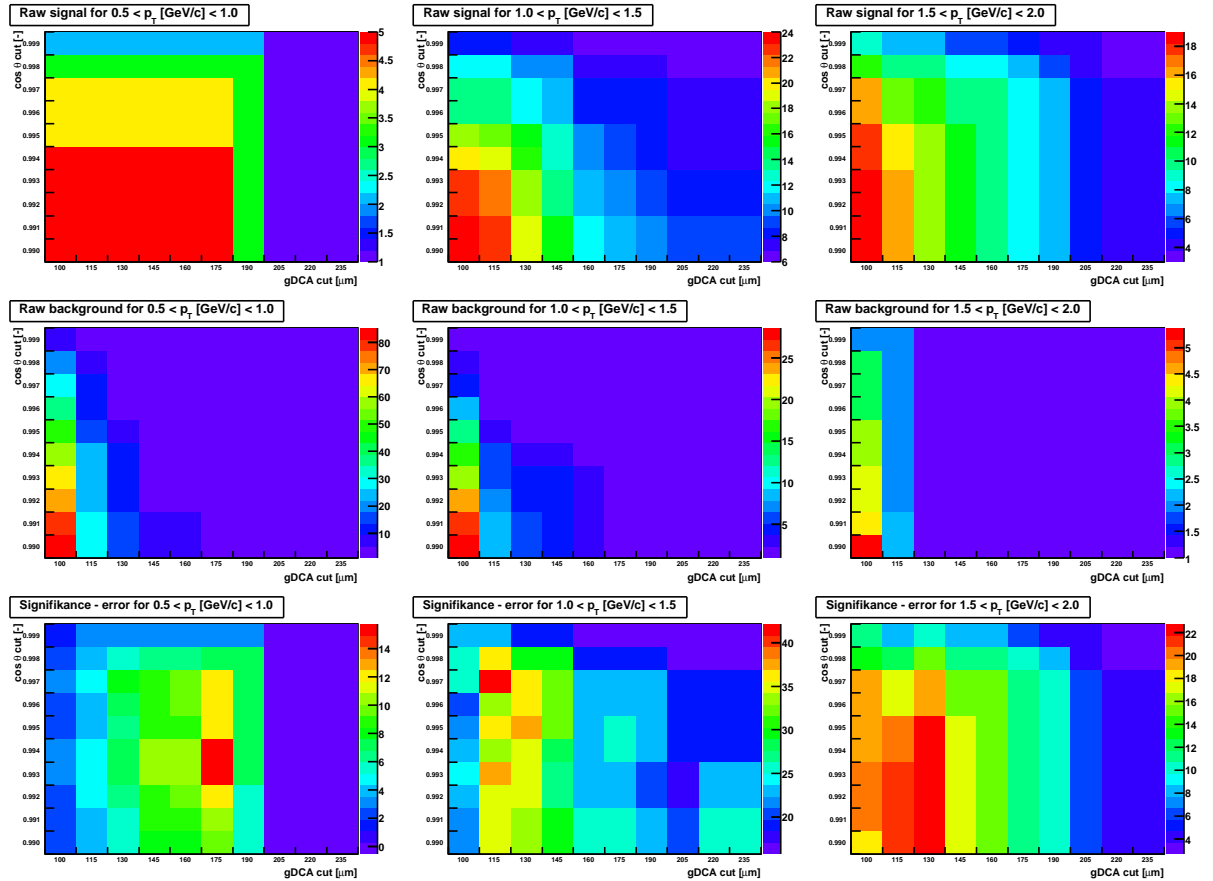


Figure 4.1: D⁺ signal and background before rescaling and significance after rescaling to 100M events as a function of gDCA and cos θ cut for three p_T ranges. ($1854 < M_{inv} < 1884$ MeV/c², good PID)

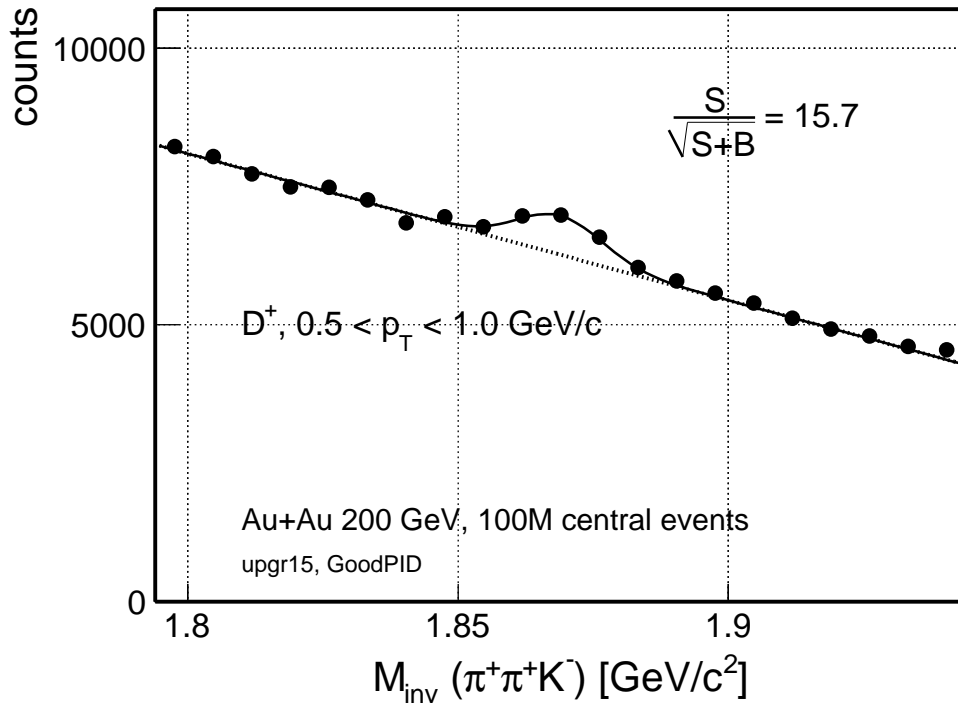


Figure 4.2: Expected D^+ signal for 100M central Au+Au collisions at $\sqrt{s_{NN}} = 200$ GeV, $0.5 < p_T < 1.0$ GeV/c, upgr15. (good PID only)

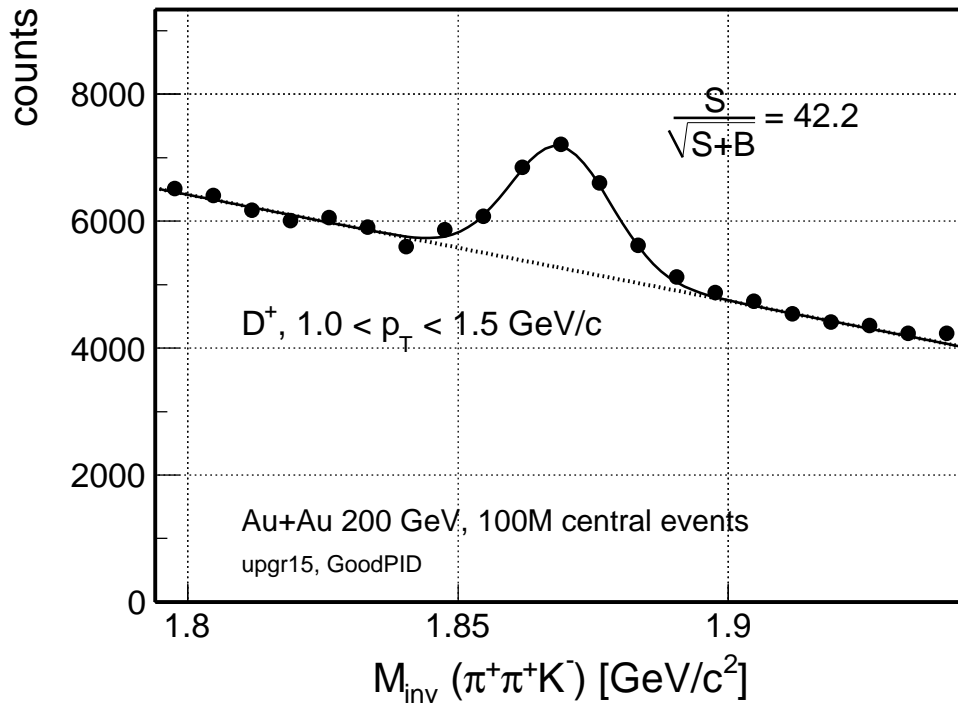


Figure 4.3: Expected D^+ signal for 100M central Au+Au collisions at $\sqrt{s_{NN}} = 200$ GeV, $1.0 < p_T < 1.5$ GeV/c, upgr15. (good PID only)

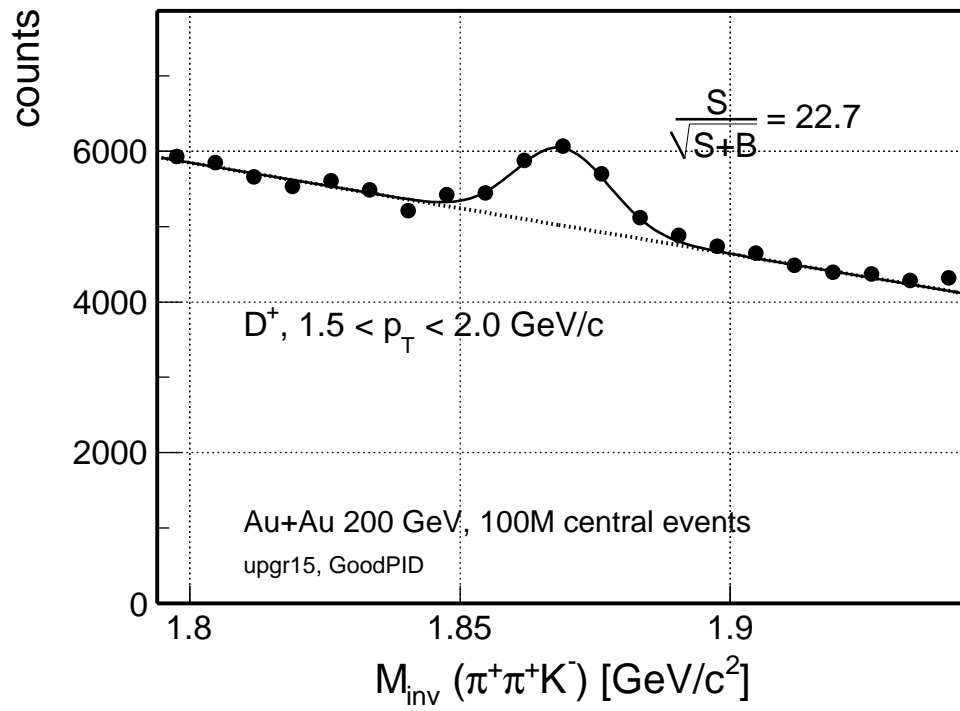


Figure 4.4: Expected D^+ signal for 100M central Au+Au collisions at $\sqrt{s_{NN}} = 200 \text{ GeV}$, $1.5 < p_T < 2.0 \text{ GeV}/c$, upgr15. (good PID only)

Conclusions

We have studied performance of the new proposed detector Heavy Flavor Tracker for STAR in direct topological reconstruction of D^+ mesons up to $p_T = 2.0$ GeV/c. In study of simulated data we have reached excellent significance of D^+ signal (see Tab. 4.1). This will further extend previously reported [5] capabilities of STAR with HFT upgrade to do precision measurements of partonic energy loss, charm collectivity and baryon/meson ratios. Systematic study of these quantities would help to understand processes, which take place in hot and dense matter created in heavy-ion collisions at RHIC.

p_T [GeV/c]	signal significance
0.5 - 1.0	15.7
1.0 - 1.5	42.2
1.5 - 2.0	22.7

Table 4.1: D^+ signal significance as a function of p_T .

These parameters of the detector can be achieved by using low mass monolithic active pixel sensors (PIXEL) for accurate spacial resolution and fast strip detector (IST) for high-level pointing resolution in the high multiplicity environment of heavy nuclei collisions with RHIC-II luminosity.

Acknowledgment

I would like to thank Mgr. Jan Kapitán for invaluable help and guidance during creation of this work. I would like to thank also my supervisor Mgr. Jaroslav Bielčík, PhD. for his worth hints, which helped to improve the research project.

Bibliography

- [1] Y. L. Dokshitzer, D. E. Kharzeev, Phys. Lett. B **519**, 199 (2001).
- [2] E. Bruna, PhD Thesis, University of Torino (2007).
- [3] M. Tesař, Bachelor's Thesis, Czech Technical University in Prague (2008).
- [4] W.-M. Yao et al, Particle Physics Booklet, Journal of Physics G**33**, 1, (2006).
- [5] J. Kapitan, STAR inner tracking upgrade - a performance study, Eur. Phys. J. C **62**, 217-221 (2009).